One Pot Doxorubicin Partitioning and Encapsulation on Silica Nanoparticle, Applying Aqueous Two Phase System for Preparation of pH-Responsive Nanocarriers

Mojhdeh Baghbanbashi
Amirkabir University of Technology (Tehran Polytechnic)
Gholamreza Pazuki (ghpazuki@aut.ac.ir)
Amirkabir University of Technology (Tehran Polytechnic)
Sepideh Khoee
University of Tehran

Research Article

Keywords: Controlled release, pH-sensitive, Aqueous two-phase system, Hydrogen bonding, Silica nanoparticle, Lysine

Posted Date: July 21st, 2021

DOI: https://doi.org/10.21203/rs.3.rs-732929/v1

One Pot Doxorubicin Partitioning and Encapsulation on Silica Nanoparticle, Applying Aqueous Two Phase System for Preparation of pH-Responsive Nanocarriers

Mojhdeh Baghbanbashi [1], Gholamreza Pazuki [1,*], Sepideh Khoee [2]

[1] Department of Chemical Engineering, Amirkabir University of Technology (Tehran Polytechnic), Tehran, Iran.

[2] School of Chemistry, College of Science, University of Tehran, Tehran, Iran.

[1],* Corresponding author: Tel: +98-021-64543159. Fax: +98-021-66405847. E-mail address: ghpazuki@aut.ac.ir (G.R. Pazuki)

Abstract

Providing an efficient system for drug delivery and chemotherapy has always been an important issue. Modification of the surface of silica nanoparticles (SiO_2) provides an opportunity for achieving stimulus-sensitive drug delivery system. Here, we have modified the surface of SiO_2 using hydrogen bonding interactions by employing an aqueous two-phase system (ATPS) based on polyethylene glycol and lysine. This novel biocompatible ATPS provides an environment for simultaneous drug encapsulation, SiO_2 modification, and drug partitioning in one pot. Addition of SiO_2 to ATPS increased the partitioning of doxorubicin (DOX) as an anti-cancer drug from 47.92 in the absence of nanoparticles to 92.33 due to the interactions between drug and nanoparticles. The formation of nanoformulation and its characteristics were investigated applying microscopy, spectroscopy and thermal analysis. Drug release study demonstrated that DOX is loaded on nanoformulations efficiently with an encapsulation efficiency of 63.84% and shows lower release in physiological environment compared to the unmodified nanoparticles. While in acidic conditions of pH 5.5, significant increase was observed in the release profile. MTT assay on MCF-7 cancer cells confirmed that the nanoformulations were non-toxic and DOX-loaded nanocarrier showed anti-cancer behavior. These results indicate that the prepared nanoformulations are promising nanocarriers for controlled drug release purposes.

Keywords: Controlled release, pH-sensitive, Aqueous two-phase system, Hydrogen bonding, Silica nanoparticle, Lysine.

1 Introduction

Cancer has long been a major threat to human health, and despite many efforts and studies, it has always been a significant challenge [1,2]. Chemotherapy, as the most widely used method for cancer treatment, destroys both cancerous and normal cells and causes severe side effects [3]. On the other hand, a small portion of the introduced drug is delivered to the tumor tissues diminishing the efficiency of chemotherapy [4]. This causes the drug to be prescribed in higher doses, which leads to the systematic removal of drug from the body and is not affordable [5,6]. Drug resistance of cancers to chemotherapy is another factor that results in treatment failure [7]. To address these issues, it is necessary to design targeted drug delivery systems in order to: 1) target the tumor site and decrease the drug concentration in other tissues; 2) release the drug in response to internal or external stimuli such as redox, pH, biological molecules in the tumor environment, magnetic field, light and temperature [8-12]. Targeted nano-drug delivery systems with small sizes (10 to 100 nm) enhance permeation through the newborn blood vessels of tumor tissues with slower clearance due to the lack of lymph [12]. These drug nanocarriers including micelles [13,14], polymersomes [15], liposomes [16], dendrimers [17], carbon nanotubes [18], magnetic nanoparticles[19] and silica nanoparticles [20,21] are of high importance because of their higher permeability, detection of target cells, accumulation at cancer sites, less side effects, and more efficient treatment [4,5,22].

Silica nanoparticles (SiO_2 NP) provide many advantages, including high stability [23], biocompatibility [24,25], tumor site accumulation ability through enhanced permeability and retention (EPR) effect [26], low toxicity [27-32], simple synthesis and surface modification, uniform and adjustable morphology, easy and low-cost large-scale synthesis [33] and high surface area to volume ratio [28]. The application of SiO_2 NP, which is approved by food and drug administration (FDA) as

safe materials [34], have been widely studied in the diagnosis and treatment of diseases as imaging agents, biosensors, and drug and gene carriers [21,25,35-39].

Modification of the surface of silica nanoparticles offers opportunities to prevent nanoparticles accumulation and elimination by proteins and ions in the physiological microenvironment and barricade the burst release of the drug, which increases the level of the drug in normal tissues and reduces its concentration at the tumor site [34,40,41]. A well-investigated method to modify the surface of nanoparticles is PEGylation [42,43]. Polyethylene glycol (PEG) is an FDA approved non-toxic, non-immunogenic, and non-antigenic polymer [34,44], which forms a hydrophilic layer around the nanoparticle and increases the water solubility, and improves dispersion and colloidal stability using the stealthing effect of PEG through rapid movement of hydrated polymer chains [23,40,45,46]. PEGylation can significantly prevent protein adsorption on nanoparticle surface and rapid clearance of nanoparticles by RES that leads to increased EPR and circulation time [12].

Polymeric compounds are attached on the surface of inorganic nanocarriers in various methods, including strong chemical bonds (covalent or ion-covalent bonds), the reaction of end-functionalized-polymers with the functional groups on nanoparticles, initiation of polymerization from the surface, and physical interactions such as hydrogen bonding and Van der Waals interactions [23,47,48]. Non-covalent bonds are more sensitive to stimulus. Among these, hydrogen bonding is a selective and relatively potent interaction that occurs only between the hydrogen bond donor and receptor and is very sensitive to pH changes [49,50]. This bond has low activation energy and can occur at room temperature. The surface of silica nanoparticles is covered by silanol, which is prone to form hydrogen bondings with PEG and drugs [49,51]. So far, a considerable amount of effort has been devoted to designing pH-sensitive polymeric nanocarriers using hydrogen bonding [49,50,52,53]. Hydrogen-bonded carriers can be used to deliver drugs to tumors that have an acidic

environment. In addition, hydrogen bonding between the carrier and the drug can also prevent the immediate release of drug [49].

Another compound applied in surface modification of nanoparticles is lysine, owing to its low cost, high compatibility, and availability [54-57]. Lysine is an essential compound in the body for strengthening the calcium absorption from the gastrointestinal tract, helping bone growth, collagen and antibody production, and tissue repair. Lysine is one of the simplest essential amino acids with one amine group in its side chain prone to interact with the hydroxyl groups of the silica surface through hydrogen bonding [55-57].

Aqueous two-phase systems (ATPS) consist of an aqueous mixture of two water-soluble components [58] that are incompatible with each other and can split into two aqueous phases above a critical concentration [59,60]. This capability offers a tool for a variety of applications, including the isolation of sensitive biomolecules such as cells, enzymes, nucleic acids and proteins, encapsulation, enrichment, and delivery of active compounds and mimicry of cellular environment [17,60-64]. Due to water presence in both phases and low interfacial tension between the phases, ATPSs provide a compatible medium for biomolecules [60,65,66].

A tremendous effort has been made on PEG-based ATPSs [67,68]. However, the formation of ATPS using amino acids is less investigated. Amino acids are inner salts with a high affinity for water, and despite their weaker soluting-out ability compared to inorganic salts, they can form a benign ATPS for biological materials [60,61]. Therefore, in this research, a novel biocompatible PEG-lysine based ATPS is presented. This ATPS, as the first example of it, is employed for simultaneous partitioning and loading of doxorubicin (DOX) on silica nanoparticles, which can be modified in the presence of PEG and lysine (Figure 1). Doxorubicin is one of the most widely used drugs in treating of various cancers, which disrupts cancer cell proliferation. Loading DOX on a targeted

carrier can help to reduce its side effects on normal cells and increase its effect on cancer cells [34]. The hydroxyl, amine, and phenolic groups of doxorubicin can bound to silanol on the surface of silica through hydrogen bondings [69,70], and in acidic condition, these bonds become unstable and protonated, leading to the release of DOX. Therefore, the phase equilibrium between PEG and lysine in an aqueous medium was investigated, and then using this ATPS, the partitioning of DOX in the absence and presence of silica nanoparticles was investigated. The release of DOX from nanocarriers resulting from self-assembly of the components was studied and its toxicity effect on MCF-7 breast cancer cells was evaluated.

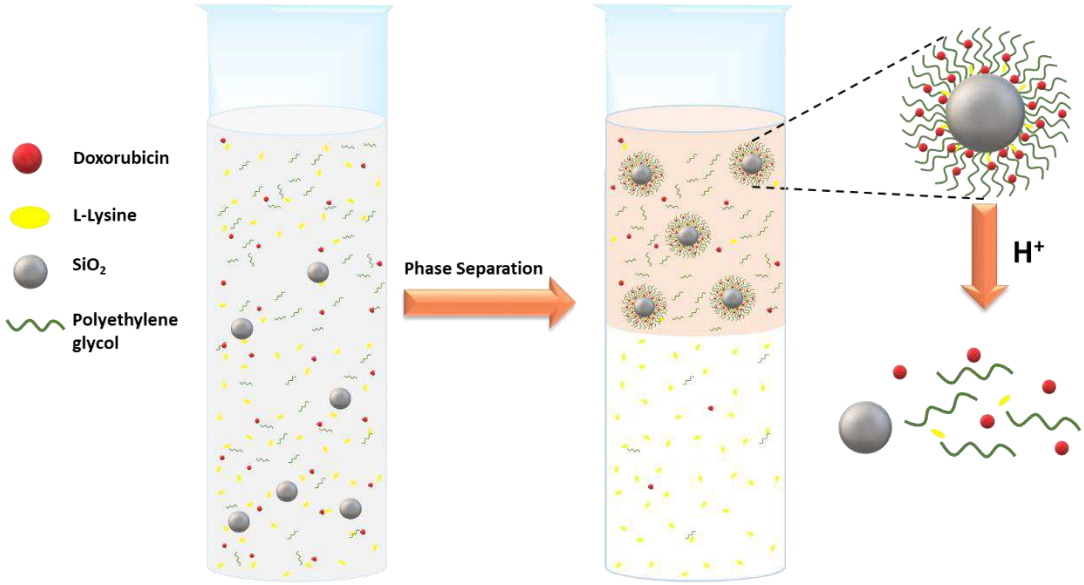

Figure 1. Schematic representation of nanocarrier formation and drug loading in PEG/lysine-based aqueous two-phase system.

2 Results and discussion

2.1 Binodal curve and tie lines

As shown in Figure 2, PEG_{6000} and lysine were able to form an aqueous two-phase system and the liquid-liquid equilibrium diagram was determined at 298 K and atmospheric pressure. Since amino

acids are weaker soluting-out induced species [60], the two-phase region is formed at higher lysine concentrations, but still represents a large immiscibility region. The Merchuk parameters were obtained by fitting the experimental binodal data (Table 1) to employ in the determination of each phase composition at different mixture points.

Various mixture points (MP) were chosen to study the partitioning of DOX in PEG_{6000}/lysine ATPS. The composition of each phase was obtained using the gravimetric method, mass balance, and the Merchuk equation (1-5), which are presented in Figure 2 and Table 2. As can be seen, the top phase is rich in PEG and lysine is dominant in the bottom phase. By increasing PEG wt%, the immiscibility increases, and at constant lysine wt%, each phase gets richer in its main component, which leads to higher *TLL*. Increasing the lysine wt% improves the phase separation as well, due to the more soluting-out effect at higher lysine concentrations. Comparing the mixture point of highest lysine wt% with highest PEG wt% and their phase compositions indicate that PEG wt% has more impact on phase separation, since the increased immiscibility resulted from higher PEG concentration is more considerable compared to the slightly increased soluting-out effect resulted from higher lysine concentration [60].

Table 1. The Merchuk parameters.

A	**B**	**$C\times10^5$**
321.2163	-0.5579	3.47

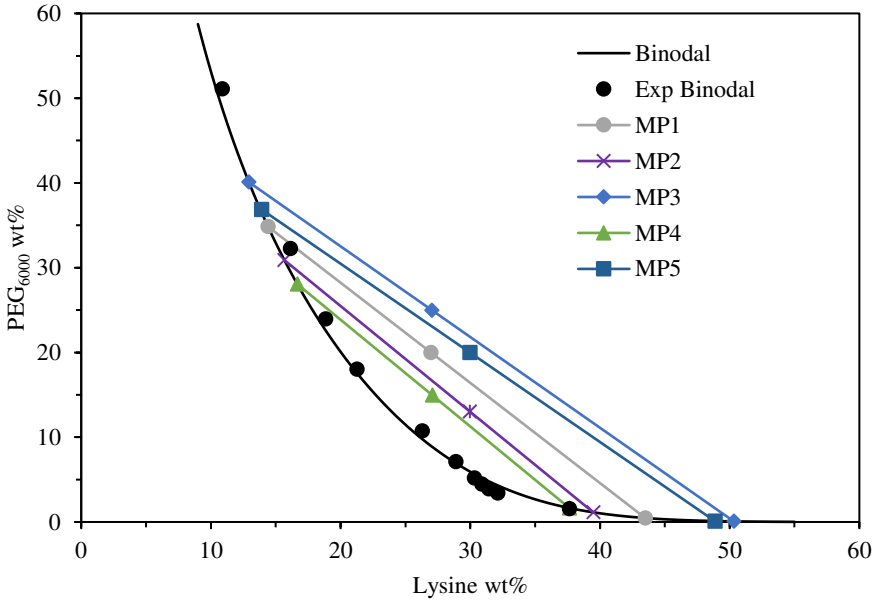

Figure 2. The phase diagram and studied mixture points (MP) and their corresponding tie lines.

Table 2. Partition coefficients of DOX and weight fraction of components in PEG_{6000}-lysine ATPS

Mixture point		Bot		Top		*TLL*	*STL*
Lys wt%	PEG wt%	Lys wt%	PEG wt%	Lys wt%	PEG wt%		
29.98	19.99	*48.88*	*0.08*	*13.89*	*36.87*	50.76	-1.05
29.97	13.02	39.48	1.14	15.67	30.89	38.11	-1.25
27.04	24.98	50.32	0.07	12.93	40.09	54.77	-1.07
26.96	20.00	43.49	0.47	14.41	34.84	45.03	-1.182
27.07	14.95	37.64	1.65	16.66	28.07	33.74	-1.26

2.2 Partitioning of DOX in PEG-lysine ATPS

The partitioning of DOX was investigated in the studied mixture points and is reported in Table 3. DOX, as a hydrophobic biomolecule (log*P*=1.41) [71] is inclined to partition to the top phase, which

is PEG-rich and possesses lower water content and hence is less hydrophilic compared to the lysine phase with higher hydrophilicity (log*P*= -3.8). According to Table 3, PEG/lysine-based ATPS has increased DOX partitioning significantly compared to the reported PEG/dextran and PEG-ran-PPG copolymer/dextran ATPSs [72]. The partition coefficient of DOX and *EE%* improved at higher PEG wt% at constant lysine wt% due to increased interactions between PEG and DOX at higher PEG amount and elevated V_r and PEG wt% in the top phase. Higher lysine wt% at constant PEG wt% in the feed improves the *TLL* and decreases *K* because of the lower water concentration in the bottom phase. According to the obtained results, higher lysine and lower PEG concentrations adversely affect DOX partitioning.

Table 3. Partition coefficient of DOX, V_r and EE%

Lysine%	PEG%	V_r	K	EE%
29.98	19.99	0.72	25.97	94.93
29.97	13.02	0.52	25.79	93.12
27.04	24.98	0.88	47.92	97.68
26.96	20.00	0.67	39.28	96.32
27.07	14.95	0.65	15.30	90.90

2.3 The effect of SiO_2 NP on DOX partitioning

SiO_2 NP was added to the ATPS mixture points with the highest and lowest DOX partition coefficients to investigate its effect on partitioning. Since 0.5 mg of SiO_2 (0.025 wt%) was added to ATPSs, the effect of the additive on binodal curve could be considered negligible [73-75]. The obtained results (Table 4) indicate that the addition of SiO_2 can increase the partitioning of DOX from 15.30 and 47.92 to 23.67 and 98.49, respectively. This improvement in DOX partition coefficient could result from the increased interactions by SiO_2 NP, which was investigated through further analysis of the separated nanoformulations obtained from the top phase.

Table 4. Partition coefficient of DOX and *EE%* in the presence of SiO_2 NP.

Lysine%	PEG%	K	EE%
26.97	24.97	92.33	98.49
26.99	14.97	23.67	94.94

2.4 FTIR analysis

The obtained nanoformulation, as well as all the components of the top phase, were analyzed through FTIR spectroscopy to investigate the effect of SiO_2, and the resulting spectrum is presented in Figure 3. In the bare SiO_2 spectrum, before water exposure, the peaks at 473, 798, and 1110 cm^{-1} are related to the siloxane network (Si-O-Si), and the peaks at 963 and 3670 cm^{-1} are assigned to silanol groups (SiOH) and hydrogen bonding in the silanol group, respectively [51,56,76,77]. The SiO_2 surface contains SiOH at room temperature, and it can be effectively hydroxylated in the presence of water and can form hydrogen bonding [51,56,78]. Due to the low activation energy of hydrogen bonding, it can occur at room temperature. While most of the peaks of SiO_2 overlap with PEG, the siloxane network can be observed at 473 and 734 cm^{-1} in the DOX@nanoformulation spectrum, confirming the presence of SiO_2. The FTIR spectrum of lysine shows a broad peak of symmetric and asymmetric groups of CH_2 and NH stretching vibration around 2500-3200 cm^{-1} [79-82], which are present in DOX@nanoformulation spectra with lower intensity. The CH band in PEG is shown at 2890 cm^{-1}, and the presence of this peak in the DOX@nanoformulation spectrum confirms the presence of PEG. The ethereal oxygen atoms in the PEG chain and its terminal hydroxyl groups can form hydrogen bonding with the silanol groups on the SiO_2 surface [47,83,84].

The broad band around the 3200-3800 cm^{-1} region indicates the formation of hydrogen bonding between the top phase components [47,79,85,86]. The peak of the carbonyl group of DOX appears at 1730 cm^{-1}, while the peaks standing for the OH of primary amine and NH appear at 3330 and 3540

cm^{-1}, respectively [87-90]. Although DOX peaks were overlapped with the signals of PEG and lysine in DOX@nanoformulation spectrum, DOX molecules can be incorporated into the complexes formed by hydrogen bonding due to the presence of phenolic, amino and hydroxyl groups in its structure, which can form hydrogen bonding, and lead to the formation of a drug-loaded nanoformulation [69,70].

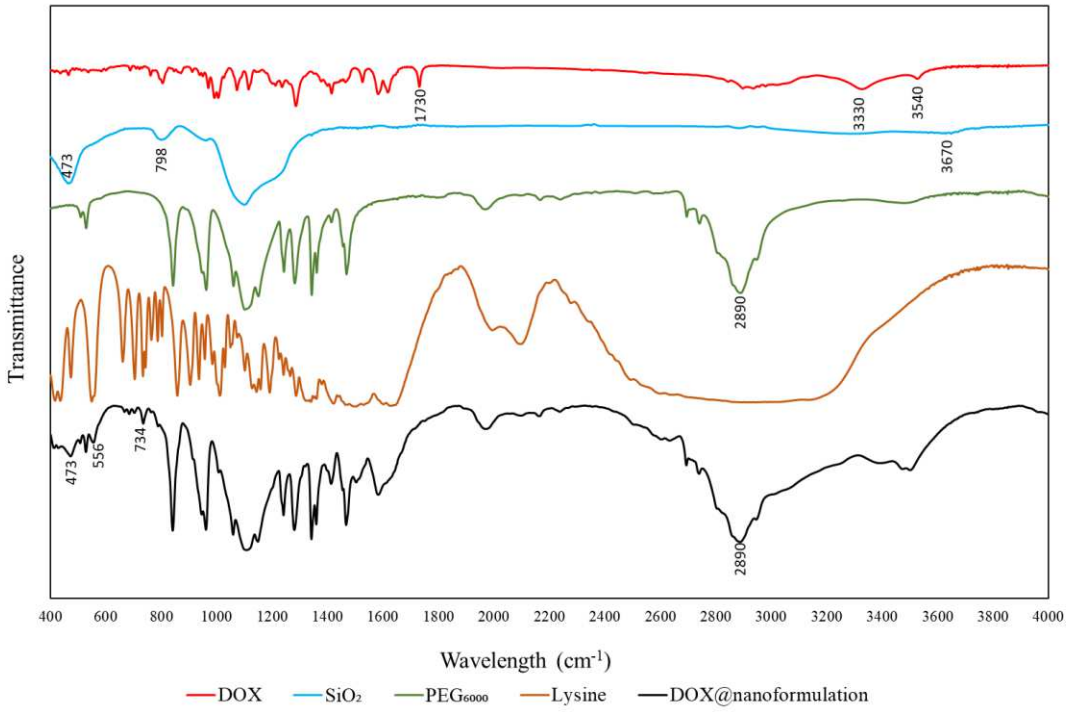

Figure 3. FTIR analysis of pure DOX, SiO_2, PEG, lysine and DOX@nanoformulation.

2.5 TGA analysis

Thermal decomposition of the obtained nanoformulation was carried out using thermal gravimetric analysis (TGA) at 25 to 600°C. Figure 4 shows the TGA thermograms of pure DOX, SiO_2, PEG, lysine and DOX@nanoformulation. The 26% mass reduction of SiO_2 around 100°C is due to physically absorbed water evaporation. The nanoformulation TGA thermogram shows a weight loss around 100°C related to water residuals. The second weight reduction occurred at 306°C. This

weight loss could be attributed to lysine presence in the top phase, which has formed hydrogen bonding to the SiOH on the silica nanoparticle surface according to the decomposition temperature range of pure lysine, which occurs at a wide temperature range (starting at about 289°C, Figure 4). The results is in accordance with the reported TGA analysis of lysine [79,91], and lysine-SiO_2 conjugates [56,57]. The subsequent decomposition appears at 327-484°C due to decomposition of PEG, which starts at higher temperatures compared to pure PEG (201°C- 510°C, Figure 4)[34]. The higher decomposition temperature of the DOX@nanoformulation thermogram confirms the formation of hydrogen bonding, which increases the thermal stability of the nanoformulation [92-94]. The last mass reduction starting at 489°C could be mainly related to DOX decomposition [95-97].

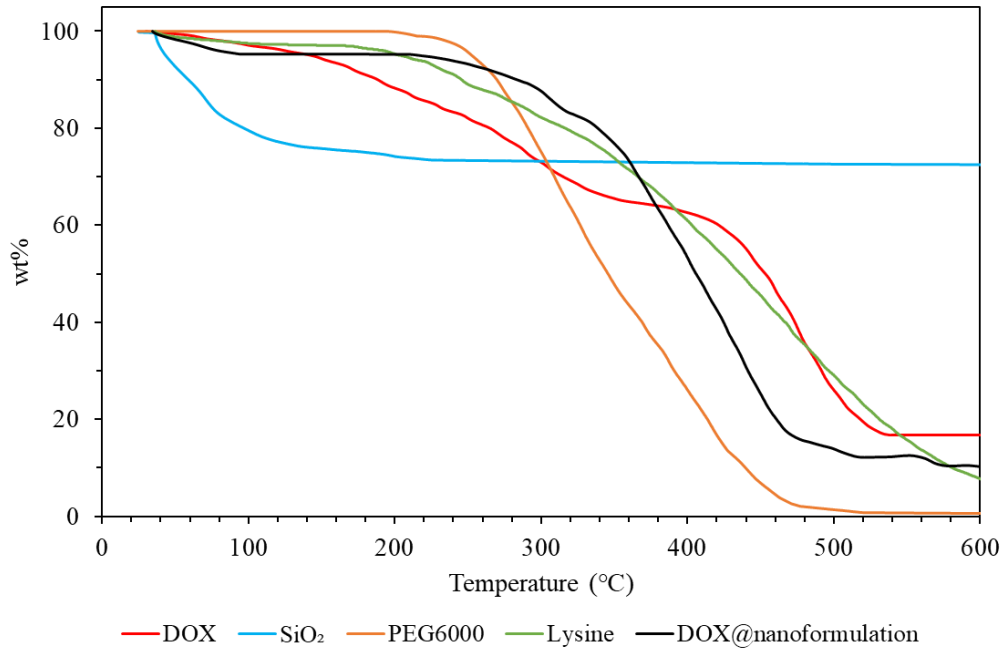

Figure 4. TGA analysis of pure DOX, SiO_2, PEG, lysine and DOX@nanoformulation.

2.6 Characterization of DOX@nanoformulation

To further analyze the properties of the nanoformulations, the hydrodynamic diameter was measured by dynamic light scattering. DLS results showed nanoparticles with the average

hydrodynamic diameter of 40.4±2.3 nm (Figure 5). TEM micrograph of the nanoparticles and TEM size distribution are shown in Figure 6. An average diameter of 25.66 nm was obtained from TEM for DOX@nanoformulations. The slightly lower diameter could be related to the TEM sample preparation procedure and dehydration of the nanoparticles [98,99].

Figure 7 shows the atomic force microscopy (AFM) images and the size histogram of the surface morphology of DOX@nanoformulation. The AFM result confirmed the formation of nanoparticles with an average diameter of 22.15 nm, which is in agreement with TEM result. The phase image of AFM (Figure 7 C) demonstrates that the surface of silica nanoparticles was modified according to the presence of different phases, which indicates the presence of different materials [100,101]. It can be observed that the nanoparticles are dispersed and do not form agglomerations. This can be attributed to surface modification, which makes the nanoparticles more stable by acting as a solvation layer and preventing interactions between SiO_2 nanoparticles [83,102,103].

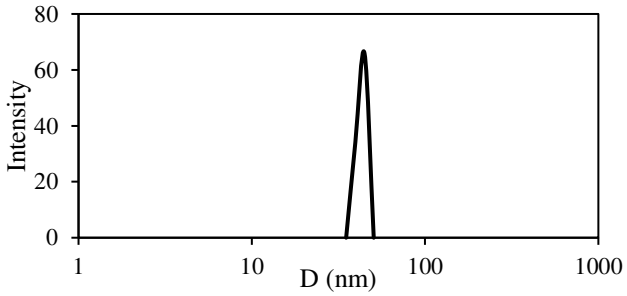

Figure 5. DLS size distribution of DOX@nanoformulation.

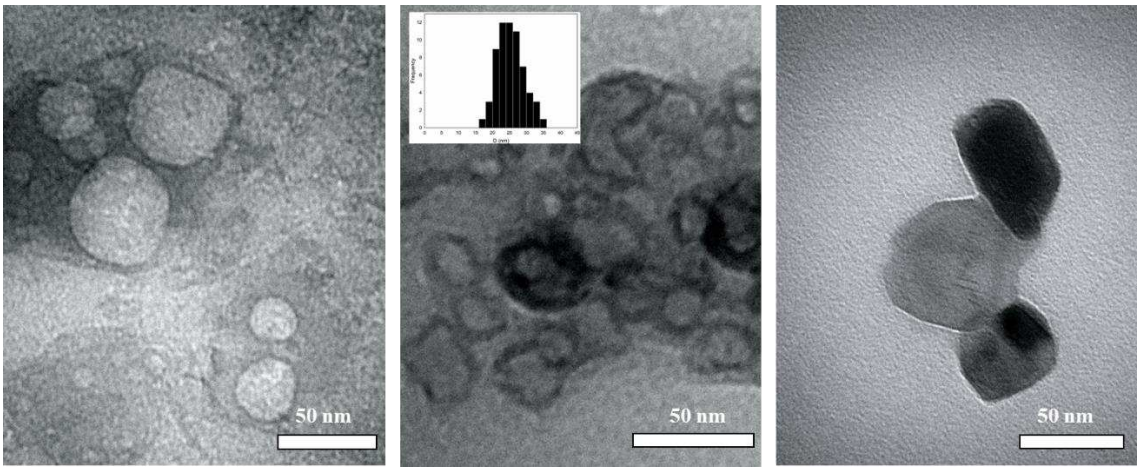

Figure 6. Transmittance electron microscopy micrograph of DOX@nanoformulation and its corresponding size histogram.

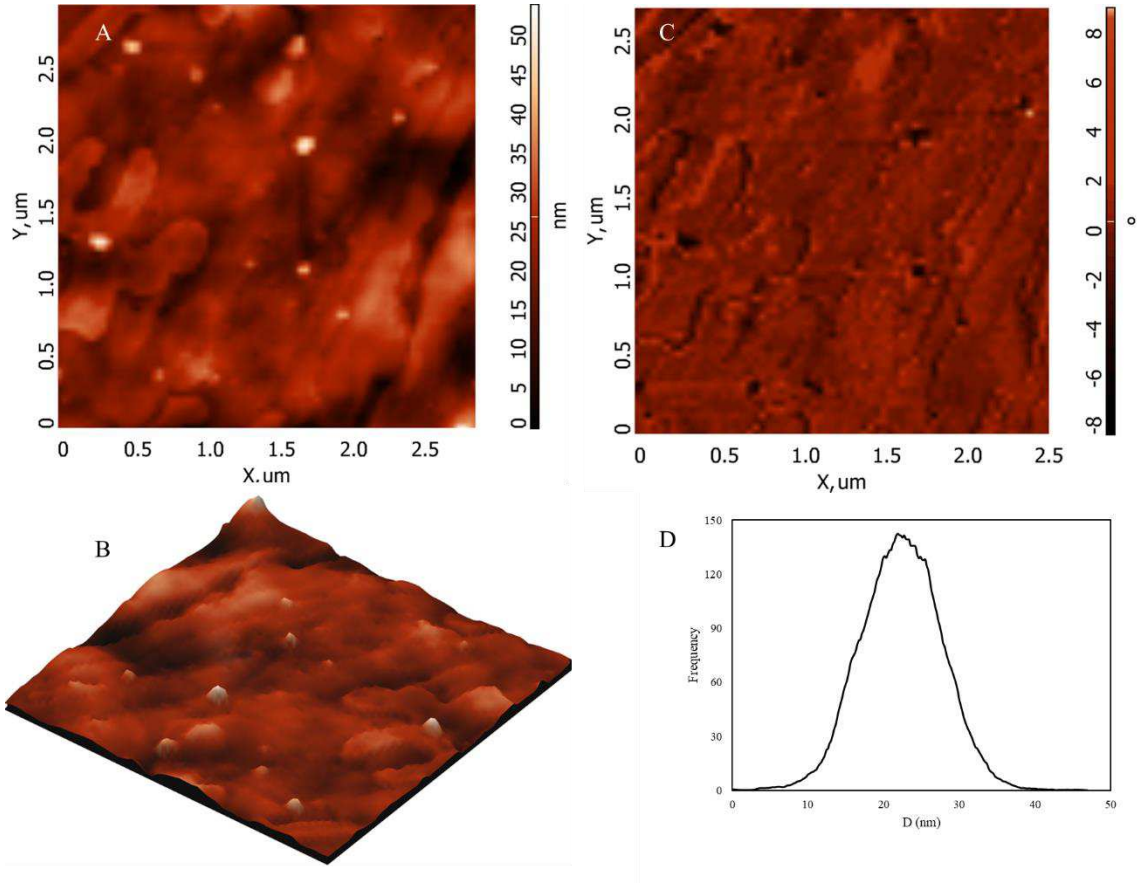

Figure 7. A) 2D and B) 3D AFM height and C) phase images of DOX@nanoformulation and D) AFM size histogram.

2.7 Drug loading and release study

Figure 8 (0 h) shows the absorbance of DOX@nanoformulation indicating that DOX was successfully loaded on the nanoformulations. As reported in Table 5, the drug encapsulation efficiency (*DE%*) and loading capacity (*LC%*) were measured by UV-Vis spectroscopy and calculated by equations (11) and (12). Surface modification has increased the drug encapsulation efficiency significantly compared to DOX@SiO_2 nanoparticles. The obtained *DE%* is in the same range as reported chemically grafted PEG-mesoporous SiO_2 nanoparticles [34]. In modified nanoparticles, in addition to the hydrogen bonding between phenolic, hydroxyl and amide groups of DOX and the abundant silanol groups on SiO_2, DOX can be trapped in the polymeric network of PEG and also forms hydrogen bonding with the PEG molecule as well, which possesses ethereal groups in its repeating unit and two terminal hydroxyl groups [69,70,83]. The slight decrease in loading capacity could be related to the considerable molecular weight of PEG_{6000} increasing the mass of the drug carrier.

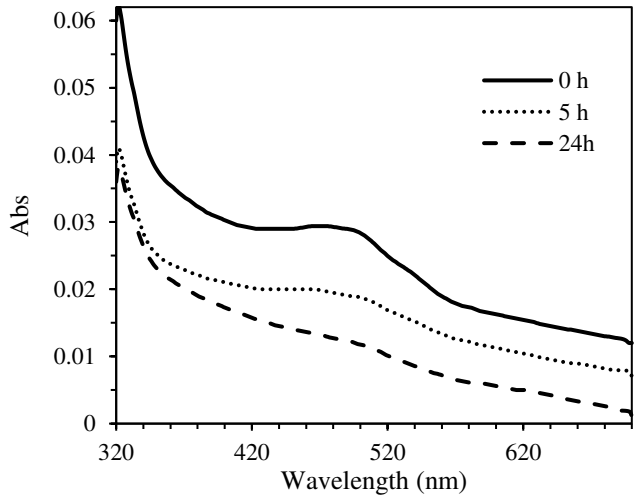

Figure 8. The absorbance of aqueous solution of DOX@nanoformulation at 0, 5 and 24 hours of dialysis in PBS.

Table 5. Drug encapsulation efficiency (*DE%*) and loading capacity (*LC%*) of DOX-loaded nanocarriers.

Carrier	*DE%*	*LC%*
SiO_2-DOX	33.15±1.78	1.19±0.06
PEG-SiO_2-DOX	63.84±2.79	0.87±0.04

Following the experiments confirming the formation of PEGylated drug carrier, the DOX@SiO_2 and DOX@nanoformulation were evaluated for their release kinetics, as represented in Figure 9. To ascertain that the drug carrier has limited the diffusion of DOX out of the structure, free drug release was also investigated. As shown, more than 99% of the free DOX was released within the first 4 hours. Compared to the free DOX, the release profile of the nanocarriers was considerably sustained at physiological pH. 35% of the drug was released at the first 5h confirming successful drug loading on PEGylated SiO_2. The decrease in the absorbance of DOX in the nanocarriers solution is related to DOX concentration decrease, which confirms the DOX release (Figure 8). 60% of DOX was released after 72h at physiological pH, and 40% remained in the carrier, suggesting the sustained and stable nanoparticle structure at pH=7.4 and good compatibility of DOX with the carrier. The release profile of DOX from bared SiO_2 nanoparticles at physiological pH was studied to investigate the effect of modification on drug release. As can be seen in Figure 9, more than 76% of DOX was released from SiO_2, indicating PEG prevention of the drug release in modified nanoparticles.

We were intrigued to study the behavior of DOX@nanoformulation at pH 5.5, which imitates the tumor environment and can affect hydrogen bonding. As can be seen in Figure 9, in acidic condition, a fast release up to 57% was obtained within 5h and 73% of the drug was released after 72h. The release profiles show that the DOX release from modified nanoparticles is pH-dependent. The acidic conditions can break hydrogen bonding by protonation of NH_2 groups on DOX and the

hydroxyl groups on SiO_2 surface. In addition, an acidic environment can increase the hydrophilicity of DOX, which improves its solubility [70,104]. The hydrogen bonding break and increased solubility of DOX led to the increased drug release from the carrier in the acidic pH.

Comparing the outcomes to the literature [34,105,106] indicates that the DOX@nanoformulation can retain the drug encapsulated in pH 7.4 and release the drug in acidic environment more efficiently, suggesting an effective pH-sensitive drug nanocarriers for DOX delivery to cancerous tissue.

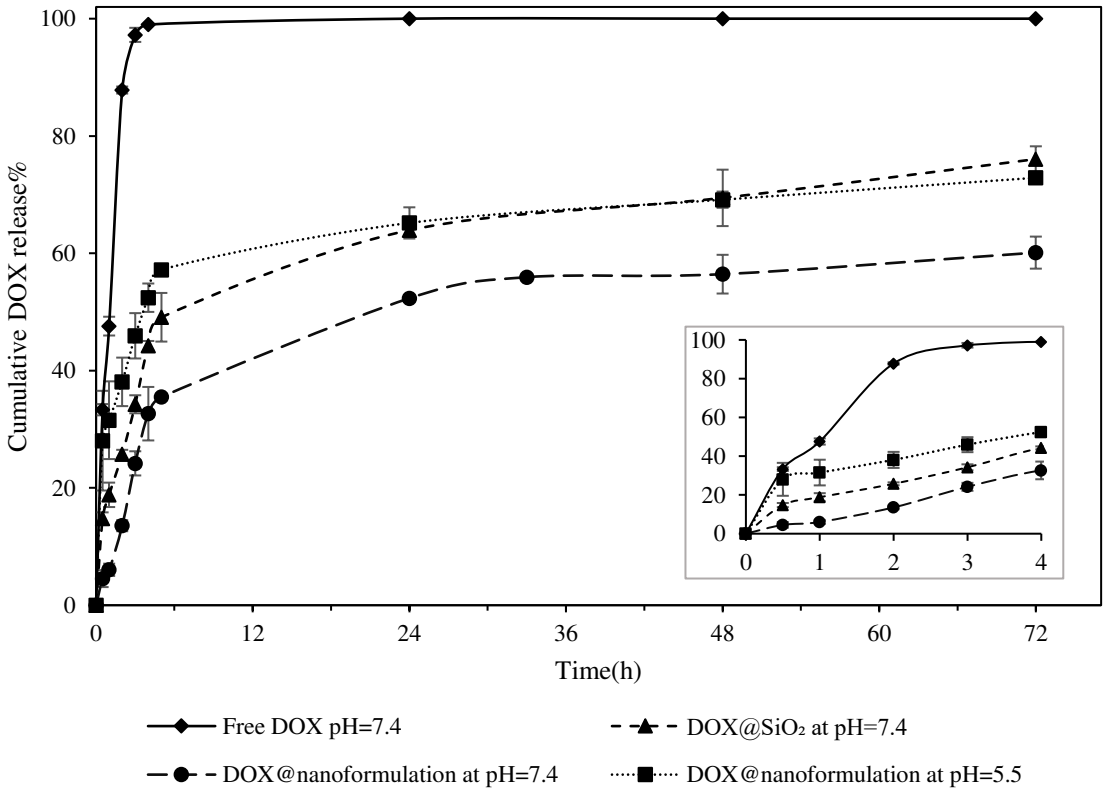

Figure 9. In vitro release profile of DOX from nanocarriers at pH 7.4 and 5.5.

2.8 Cytotoxicity assay by MTT

The cytotoxicity of the nanoformulations was evaluated by MTT assay. MCF-7 cells were treated with different concentrations of DOX, nanoformulation, and DOX@nanoformulation for 48h. The nanoformulation revealed to be non-toxic. As shown in Figure 10, the cell viability was 76.09%

of control even up to a concentration of 1000µg/mL, confirming that the prepared carrier is biocompatible and safe for drug delivery applications. DOX@nanoformulation showed cytotoxicity at concentrations higher than 62.5µg/mL, which carries 0.5µg/mL DOX. Considering the partial release of DOX from nanoformulations after 48h at pH=7.4, almost the same toxicity as free DOX was obtained. This observation proves that the DOX activity is retained after drug loading. The viability of MCF-7 cells decreased as the concentration of the carrier increased. However, the viability could be affected by the slow release of DOX from the carrier at the physiological pH.

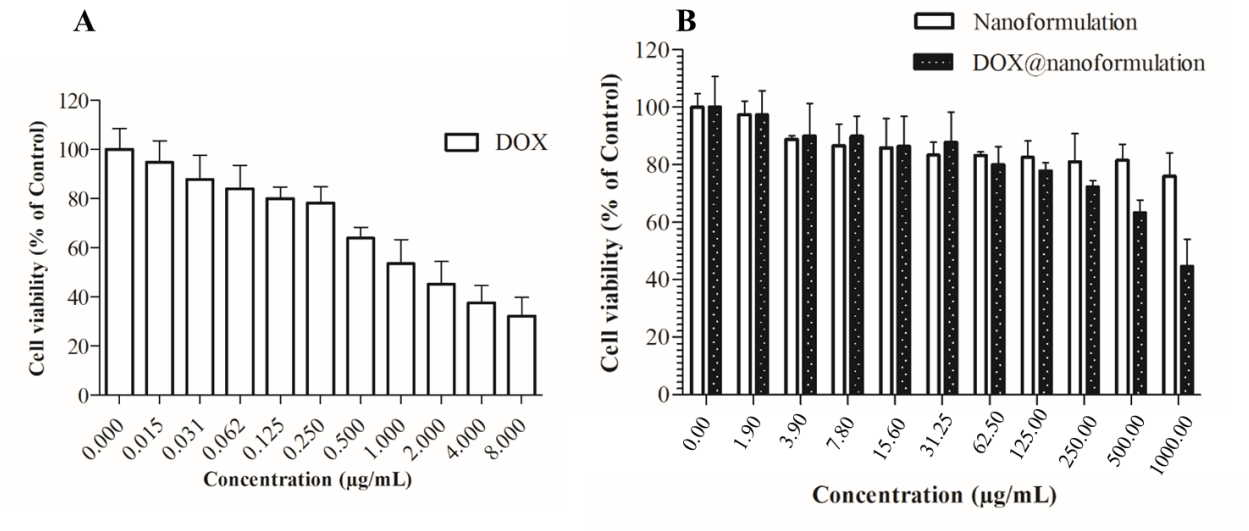

Figure 10. MTT assay of MCF-7 cell viability after treating with A) DOX, B) nanoformulation, and DOX@nanoformulation for 48h at various concentrations.

3 Material and methods

3.1 Materials and instruments

Polyethylene glycol 6000 (PEG), L-lysine monohydrochloride and dimethyl sulfoxide (DMSO) were supplied by Merck. Doxorubicin hydrochloride EP (DOX) was purchased from Synbias

Pharma. Silicon dioxide (SiO_2) nanopowder (5-15nm) was acquired from Sigma Aldrich. Human breast cancer MCF-7 cell line was supplied from the Pasteur Institute Cell Bank of Iran. A culture medium of 89% RPMI-1640 containing 10% FBS serum (Biowest) and 1% Penicillin-Streptomycin (100X) (Biowest) was prepared under sterile conditions and kept at 4°C for cell growth and maintenance. Before application, the culture medium temperature was reached to 37°C. 3-[4,5 dimethylthiazol-2-yl]-2,5-diphenyl tetrazolium bromide (MTT) was obtained from Carl Roth (Karlsruhe, Germany).

Fourier-transform infrared (FTIR) spectra were recorded on a shimadzu IR prestige 21 spectrometer at 298K. The spectra were taken on KBr discs at the range of 400-4000 cm^{-1}. Thermal analysis of the samples was explored through thermal gravimetric analysis with a heating rate of 10°C/min (TGA, TGA-50, Shimadzu). A UV-Vis Spectrophotometer (DR3900, HACH, USA) was applied to determine the drug concentration. Aqueous solutions of SiO_2 nanoparticle were sonicated using an ultrasonic bath (FALC, Italy). SZ-100z dynamic light scattering (DLS) analyzer (Horiba Jobin Jyovin) was used to measure the hydrodynamic diameter. The apparatus was equipped with a 10mW solid-state laser diode operating at λ = 532nm. Transmission electron microscopy (TEM) studies were performed with a Philips EM 208S instrument at a voltage of 100 kV. Aqueous samples were dropped on carbon-coated copper grids and then dried at 298K before analysis. Tapping mode atomic force microscopy (AFM, Ntegra, NT-MDT) measurements were carried out in air at 298K.

3.2 Phase diagram and tie lines

The binodal curves were determined through cloud point titration method as explained in literature [59,107] at 298K and atmospheric pressure. Briefly, aqueous solutions of lysine at 40 wt% and PEG

at 50 wt% were prepared gravimetrically (±10^{-4} g). The PEG solution was added dropwise to the lysine solution until the appearance of turbidity leading to the first point of binodal curve, which indicates the beginning of phase separation. The turbidity is removed by adding water and the procedure is repeated. The Merchuk equation [108] was applied to correlate the obtained binodal data.

$$[PEG] = A \exp\left(B [Lys]^{0.5} - C [Lys]^3\right) \quad (1)$$

A, B and C are the constants obtained by regression of binodal data. The phase compositions were obtained applying gravimetric method and Merchuk equation [72,109].

$$[PEG]_{Top} = A \exp\left(B [Lys]_{Top}^{0.5} - C [Lys]_{Top}^3\right) \quad (2)$$

$$[PEG]_{Bot} = A \exp\left(B [Lys]_{Bot}^{0.5} - C [Lys]_{Bot}^3\right) \quad (3)$$

$$[PEG]_{Top} = \frac{[PEG]_F}{\alpha} - \frac{1-\alpha}{\alpha}[PEG]_{Bot} \quad (4)$$

$$[Lys]_{Top} = \frac{[Lys]_F}{\alpha} - \frac{1-\alpha}{\alpha}[Lys]_{Bot} \quad (5)$$

Where the subscripts *Top* and *Bot* refer to the top and bottom phases, respectively. The tie line length and the slope of the tie lines were calculated using equations (6) and (7), respectively.

$$TLL = \sqrt{\left([Lys]_{Top} - [Lys]_{Bot}\right)^2 + \left([PEG]_{Top} - [PEG]_{Bot}\right)^2} \quad (6)$$

$$STL = \frac{[PEG]_{Top} - [PEG]_{Bot}}{[Lys]_{Top} - [Lys]_{Bot}} \quad (7)$$

3.3 Partitioning of doxorubicin

Partitioning of doxorubicin was investigated through an established procedure [59,110]. Briefly, ATPSs composed of various concentrations of PEG, lysine, and deionized water (DIW) containing 0.05mg of doxorubicin were prepared gravimetrically (u(m)=10^{-4} g) at 298K and atmospheric pressure. The solutions were stirred vigorously and were left for 24h to reach equilibrium and were subsequently centrifuged at 2700 rpm for 15min to acquire well phase-separated ATPSs. The phases were separated intently, and the mass and volume of each phase were measured. The drug concentration in each phase was obtained by analyzing samples of each phase using the calibration curve and UV-Vis analysis at 481nm. Since the samples were diluted by DIW and other components do not show absorption at visible wavelengths, DIW was used as blank, and all experiments were performed with three replications. The partition coefficient of doxorubicin (K), extraction efficiency ($EE\%$), and the volume ratio (V_r) were determined using the following equations.

$$K = \frac{[DOX]_{Top}}{[DOX]_{Bot}} \quad (8)$$

$$EE\% = \frac{m(DOX)_{top}}{m(DOX)_{total}} \times 100 \quad (9)$$

$$V_r = \frac{V_{Top}}{V_{Bot}} \quad (10)$$

3.4 Partitioning of DOX in the presence of SiO_2 and drug loading

The same procedure was applied to investigate the partitioning of doxorubicin in the presence of SiO_2. Briefly, an aqueous solution of SiO_2 (200mg/mL) was sonicated for 1h. The drug was added to the solution and it was sonicated for 30 more minutes. The ATPS mixture points were prepared

by adding the desired amount of PEG and lysine and the solutions were stirred vigorously. The ratio of SiO_2/DOX was kept at 10 in all samples. As before, to measure the partitioning of the DOX in the presence of SiO_2, the two phases were separated carefully, and the DOX absorbance was measured by UV-Vis spectrophotometer.

3.5 Characterization of nanoformulations

In order to separate the drug-loaded PEG/lysine coated SiO_2 nanoformulation, the top phase was centrifuged at 10000rpm for 30min and the supernatant was decanted. The sediment was dried under vacuum and characterized and analyzed using TGA and FTIR. The size of nanoformulations was measured in aqueous solutions by DLS and the morphology was determined through microscopic observation methods of TEM and AFM. The drug encapsulation efficiency (*DE%*) and loading capacity (*LC%*) were obtained using UV-Vis spectroscopy measurement and the following equations.

$$DE\,\% = \frac{\text{mass}_{\text{Loaded drug}}}{\text{mass}_{\text{Total drug}}} \times 100 \tag{11}$$

$$LC\,\% = \frac{\text{mass}_{\text{Loaded drug}}}{\text{mass}_{\text{Total drug}} + \text{mass}_{\text{Polymer}}} \times 100 \tag{12}$$

3.6 Drug release

The dialysis tubing method was employed to study the drug release profiles with three replicates [13]. 20 mg of DOX@nanoformulation or DOX@SiO_2 was dissolved in 2ml DIW and placed in 6 kDa MWCO dialysis tubing and dialyzed against 140mL saline phosphate buffer (PBS) and 1% v/v Tween 80 with pH = 7.4 and 5.5. At specified time intervals, 20 μL samples were taken from

dialysis tubing. The samples were diluted and the unreleased drug concentration was measured by UV-Vis spectroscopy.

3.7 Cell proliferation assay

MTT assay was employed to study the cytotoxic effect of free drug, blank nanocarriers, and drug-loaded nanocarrier [111,112]. 10^4 cells of MCF-7 were cultured on each well of 96-well plates and were incubated for 24h. Afterward, the medium was replaced with mediums containing 100 µL of DOX, nanoformulation, and DOX@nanoformulation at various concentrations. After 48h of incubation, the medium was removed carefully and 20 µL of MTT solution in PBS (5mg/mL) was added. The plate was incubated for 4 h at 37°C in darkness. Upon completion, 100 µL of DMSO was added to each well and the plate was shaken for 20min to dissolve the formed formazan crystals through the metabolic activity of mitochondria of live cells. The salts concentration quantification was performed using spectrophotometry analysis and measuring the absorbance of the samples at 570 nm and 690 nm (as the reference wavelength). All experiments were performed in three replicates.

4 Conclusion

The possibility of developing a method for simultaneous nanocarrier preparation and drug encapsulation can notably influence the practicability, efficacy, and accessibility of drug carriers. We employed a new aqueous two-phase system based on polyethylene glycol and lysine (as an essential amino acid in the human body) to investigate the partitioning of DOX, which is an important parameter in purification processes. The addition of silica nanoparticles to the ATPS increased the doxorubicin partitioning considerably, suggesting strong interactions in the system.

Analyzing the obtained assemblies showed that due to the formation of hydrogen bonding between the components in the system, including DOX, SiO_2, PEG, and lysine, which are all prone to form this non-covalent bonding, drug loading and SiO_2 surface modification can occur at the same time. The formed biocompatible nanocarrier offers an encapsulation efficiency of 63.84%. Investigation of the release profile of the nanocarriers showed that the surface modification prevented the drug escape and showed a more stable release compared to the bare DOX-loaded SiO_2. Evaluation of drug release in acidic conditions indicated that the hydrogen bondings between components were pH-responsive and accelerated drug release. Evaluation of the toxicity of this carrier on MCF-7 breast cancer cells demonstrated that the nanocarriers had no cytoxicity and encapsulation of the drug showed high anti-cancer efficacy. The obtained results suggest that a biocompatible ATPS can be applied for simultaneous drug partitioning and loading and is a promising method for drug delivery purposes.

Author contributions

Mojhdeh Baghbanbashi: Conceptualization; Data curation; Investigation; Methodology; Validation; Visualization; Writing - original draft. **Gholamreza Pazuki:** Conceptualization; Validation; Supervision; Writing - review & editing. **Sepideh Khoee:** Validation; Supervision; Writing - review & editing.

Competing interests

The authors declare no competing interests.

5 References

1 Waks, A. G. & Winer, E. P. Breast Cancer Treatment: A Review. *JAMA* **321**, 288-300, doi:10.1001/jama.2018.19323 (2019).

2 Lee, S. Y., Kang, M. S., Jeong, W. Y., Han, D.-W. & Kim, K. S. Hyaluronic Acid-Based Theranostic Nanomedicines for Targeted Cancer Therapy. *Cancers* **12**, 940 (2020).

3 Tu, X. *et al.* Efficient cancer ablation by combined photothermal and enhanced chemo-therapy based on carbon nanoparticles/doxorubicin@SiO2 nanocomposites. *Carbon* **97**, 35-44, doi:https://doi.org/10.1016/j.carbon.2015.05.043 (2016).

4 Wan, L. *et al.* A novel intratumoral pH/redox-dual-responsive nanoplatform for cancer MR imaging and therapy. *Journal of Colloid and Interface Science* **573**, 263-277, doi:https://doi.org/10.1016/j.jcis.2020.04.026 (2020).

5 Bahrami, B. *et al.* Nanoparticles and targeted drug delivery in cancer therapy. *Immunol. Lett.* **190**, 64-83, doi:https://doi.org/10.1016/j.imlet.2017.07.015 (2017).

6 Gao, Z., Zhang, L., Hu, J. & Sun, Y. Mesenchymal stem cells: a potential targeted-delivery vehicle for anti-cancer drug loaded nanoparticles. *Nanomedicine: Nanotechnology, Biology and Medicine* **9**, 174-184, doi:https://doi.org/10.1016/j.nano.2012.06.003 (2013).

7 Muley, H., Fadó, R., Rodríguez-Rodríguez, R. & Casals, N. Drug uptake-based chemoresistance in breast cancer treatment. *Biochemical Pharmacology* **177**, 113959, doi:https://doi.org/10.1016/j.bcp.2020.113959 (2020).

8 Alsehli, M. Polymeric nanocarriers as stimuli-responsive systems for targeted tumor (cancer) therapy: Recent advances in drug delivery. *Saudi Pharmaceutical Journal* **28**, 255-265, doi:https://doi.org/10.1016/j.jsps.2020.01.004 (2020).

9 Mi, P. Stimuli-responsive nanocarriers for drug delivery, tumor imaging, therapy and theranostics. *Theranostics* **10**, 4557-4588, doi:10.7150/thno.38069 (2020).

10 Mura, S., Nicolas, J. & Couvreur, P. Stimuli-responsive nanocarriers for drug delivery. *Nat. Mater.* **12**, 991, doi:10.1038/nmat3776 (2013).

11 Ganta, S., Devalapally, H., Shahiwala, A. & Amiji, M. A review of stimuli-responsive nanocarriers for drug and gene delivery. *J. Controlled Release* **126**, 187-204, doi:https://doi.org/10.1016/j.jconrel.2007.12.017 (2008).

12 Zhang, Q., Zhao, H., Li, D., Liu, L. & Du, S. A surface-grafted ligand functionalization strategy for coordinate binding of doxorubicin at surface of PEGylated mesoporous silica nanoparticles: Toward pH-responsive drug delivery. *Colloids Surf., B* **149**, 138-145, doi:https://doi.org/10.1016/j.colsurfb.2016.10.018 (2017).

13 Lotocki, V. *et al.* Miktoarm Star Polymers with Environment-Selective ROS/GSH Responsive Locations: From Modular Synthesis to Tuned Drug Release through Micellar Partial Corona Shedding and/or Core Disassembly. *Macromol. Biosci.* **21**, 2000305, doi:https://doi.org/10.1002/mabi.202170005 (2021).

14 Cheng, C.-C. *et al.* Hydrogen-bonded supramolecular micelle-mediated drug delivery enhances the efficacy and safety of cancer chemotherapy. *Polym. Chem.* **11**, 2791-2798, doi:10.1039/D0PY00082E (2020).

15 Zavvar, T. *et al.* Synthesis of multimodal polymersomes for targeted drug delivery and MR/fluorescence imaging in metastatic breast cancer model. *Int. J. Pharm.* **578**, 119091, doi:https://doi.org/10.1016/j.ijpharm.2020.119091 (2020).

16 Li, J. *et al.* Recent Advancements in Liposome-Targeting Strategies for the Treatment of Gliomas: A Systematic Review. *ACS Applied Bio Materials* **3**, 5500-5528, doi:10.1021/acsabm.0c00705 (2020).

17 Adeli, M., Fard, A. K., Abedi, F., Chegeni, B. K. & Bani, F. Thermo- and pH-sensitive dendrosomes as bi-phase drug delivery systems. *Nanomedicine: Nanotechnology, Biology and Medicine* **9**, 1203-1213, doi:https://doi.org/10.1016/j.nano.2013.05.013 (2013).

18 Faraji Dizaji, B., Khoshbakht, S., Farboudi, A., Azarbaijan, M. H. & Irani, M. Far-reaching advances in the role of carbon nanotubes in cancer therapy. *Life Sci.* **257**, 118059, doi:https://doi.org/10.1016/j.lfs.2020.118059 (2020).

19 Farzin, A., Etesami, S. A., Quint, J., Memic, A. & Tamayol, A. Magnetic Nanoparticles in Cancer Therapy and Diagnosis. *Adv. Healthc. Mater.* **9**, 1901058, doi:https://doi.org/10.1002/adhm.201901058 (2020).

20 Gao, Y., Gao, D., Shen, J. & Wang, Q. A Review of Mesoporous Silica Nanoparticle Delivery Systems in Chemo-Based Combination Cancer Therapies. *Front. Chem.* **8**, 1086 (2020).

21 Wu, X., Wu, M. & Zhao, J. X. Recent development of silica nanoparticles as delivery vectors for cancer imaging and therapy. *Nanomedicine: Nanotechnology, Biology and Medicine* **10**, 297-312, doi:https://doi.org/10.1016/j.nano.2013.08.008 (2014).

22 Gu, J. *et al.* Targeted doxorubicin delivery to liver cancer cells by PEGylated mesoporous silica nanoparticles with a pH-dependent release profile. *Microporous Mesoporous Mater.* **161**, 160-167, doi:https://doi.org/10.1016/j.micromeso.2012.05.035 (2012).

23 Yagüe, C., Moros, M., Grazú, V., Arruebo, M. & Santamaría, J. Synthesis and stealthing study of bare and PEGylated silica micro- and nanoparticles as potential drug-delivery vectors. *Chemical Engineering Journal* **137**, 45-53, doi:https://doi.org/10.1016/j.cej.2007.07.088 (2008).

24 Abeer, M. M. *et al.* Silica nanoparticles: A promising platform for enhanced oral delivery of macromolecules. *J. Controlled Release* **326**, 544-555, doi:https://doi.org/10.1016/j.jconrel.2020.07.021 (2020).

25 Jung, H.-S., Moon, D.-S. & Lee, J.-K. Quantitative Analysis and Efficient Surface Modification of Silica Nanoparticles. *Journal of Nanomaterials* **2012**, 593471, doi:10.1155/2012/593471 (2012).

26 Vares, G. *et al.* Functionalized mesoporous silica nanoparticles for innovative boron-neutron capture therapy of resistant cancers. *Nanomedicine: Nanotechnology, Biology and Medicine* **27**, 102195, doi:https://doi.org/10.1016/j.nano.2020.102195 (2020).

27 Kim, M. *et al.* An Evaluation of the in vivo Safety of Nonporous Silica Nanoparticles: Ocular Topical Administration versus Oral Administration. *Scientific Reports* **7**, 8238, doi:10.1038/s41598-017-08843-9 (2017).

28 Kim, J.-Y. *et al.* Safety of Nonporous Silica Nanoparticles in Human Corneal Endothelial Cells. *Scientific Reports* **7**, 14566, doi:10.1038/s41598-017-15247-2 (2017).

29 Mohammadpour, R. *et al.* One-year chronic toxicity evaluation of single dose intravenously administered silica nanoparticles in mice and their Ex vivo human hemocompatibility. *J. Controlled Release* **324**, 471-481, doi:https://doi.org/10.1016/j.jconrel.2020.05.027 (2020).

30 Yu, T., Hubbard, D., Ray, A. & Ghandehari, H. In vivo biodistribution and pharmacokinetics of silica nanoparticles as a function of geometry, porosity and surface characteristics. *J. Controlled Release* **163**, 46-54, doi:https://doi.org/10.1016/j.jconrel.2012.05.046 (2012).

31 Casalini, T. Not only in silico drug discovery: Molecular modeling towards in silico drug delivery formulations. *J. Controlled Release* **332**, 390-417, doi:https://doi.org/10.1016/j.jconrel.2021.03.005 (2021).

32 Mohammadpour, R., Yazdimamaghani, M., Cheney, D. L., Jedrzkiewicz, J. & Ghandehari, H. Subchronic toxicity of silica nanoparticles as a function of size and porosity. *J. Controlled Release* **304**, 216-232, doi:https://doi.org/10.1016/j.jconrel.2019.04.041 (2019).

33 Tang, L. & Cheng, J. Nonporous silica nanoparticles for nanomedicine application. *Nano Today* **8**, 290-312, doi:https://doi.org/10.1016/j.nantod.2013.04.007 (2013).

34 Tram Nguyen, T. N. *et al.* Surface PEGylation of hollow mesoporous silica nanoparticles via aminated intermediate. *Progress in Natural Science: Materials International* **29**, 612-616, doi:https://doi.org/10.1016/j.pnsc.2019.10.002 (2019).

35 Bhakta, G. *et al.* Multifunctional silica nanoparticles with potentials of imaging and gene delivery. *Nanomedicine: Nanotechnology, Biology and Medicine* **7**, 472-479, doi:https://doi.org/10.1016/j.nano.2010.12.008 (2011).

36 Yazdimamaghani, M., Moos, P. J. & Ghandehari, H. Global gene expression analysis of macrophage response induced by nonporous and porous silica nanoparticles. *Nanomedicine: Nanotechnology, Biology and Medicine* **14**, 533-545, doi:https://doi.org/10.1016/j.nano.2017.11.021 (2018).

37 Mochizuki, C., Nakamura, J. & Nakamura, M. Development of Non-Porous Silica Nanoparticles towards Cancer Photo-Theranostics. *Biomedicines* **9**, 73 (2021).

38 Yang, Y. & Yu, C. Advances in silica based nanoparticles for targeted cancer therapy. *Nanomedicine: Nanotechnology, Biology and Medicine* **12**, 317-332, doi:https://doi.org/10.1016/j.nano.2015.10.018 (2016).

39 Parveen, S., Misra, R. & Sahoo, S. K. Nanoparticles: a boon to drug delivery, therapeutics, diagnostics and imaging. *Nanomedicine: Nanotechnology, Biology and Medicine* **8**, 147-166 (2012).

40 Zhang, Q., Ye, Z., Wang, S.-T. & Yin, J. Facile one-pot synthesis of PEGylated monodisperse mesoporous silica nanoparticles with controllable particle sizes. *Chinese Chemical Letters* **25**, 257-260, doi:https://doi.org/10.1016/j.cclet.2013.11.002 (2014).

41 Karakoti, A. S., Das, S., Thevuthasan, S. & Seal, S. PEGylated Inorganic Nanoparticles. *Angew. Chem. Int Ed.* **50**, 1980-1994, doi:https://doi.org/10.1002/anie.201002969 (2011).

42 Gal, N. *et al.* Interaction of size-tailored pegylated iron oxide nanoparticles with lipid membranes and cells. *ACS Biomater. Sci. Eng.* **3**, 249-259 (2017).

43 Ahrén, M. *et al.* Synthesis and characterization of PEGylated Gd2O3 nanoparticles for MRI contrast enhancement. *Langmuir* **26**, 5753-5762 (2010).

44 Pourjavadi, A. & Tehrani, Z. M. Mesoporous silica nanoparticles (MCM-41) coated PEGylated chitosan as a pH-responsive nanocarrier for triggered release of erythromycin. *International Journal of Polymeric Materials and Polymeric Biomaterials* **63**, 692-697 (2014).

45 Bagheri, E. *et al.* Silica based hybrid materials for drug delivery and bioimaging. *J. Controlled Release* **277**, 57-76, doi:https://doi.org/10.1016/j.jconrel.2018.03.014 (2018).

46 von Baeckmann, C., Kählig, H., Lindén, M. & Kleitz, F. On the importance of the linking chemistry for the PEGylation of mesoporous silica nanoparticles. *Journal of Colloid and Interface Science* **589**, 453-461, doi:https://doi.org/10.1016/j.jcis.2020.12.004 (2021).

47 Catauro, M., Bollino, F., Papale, F., Gallicchio, M. & Pacifico, S. Influence of the polymer amount on bioactivity and biocompatibility of SiO2/PEG hybrid materials synthesized by sol–gel technique. *Materials Science and Engineering: C* **48**, 548-555, doi:https://doi.org/10.1016/j.msec.2014.12.035 (2015).

48 Guo, T.-Y., Liu, P., Zhu, J.-W., Song, M.-D. & Zhang, B.-H. Well-defined lactose-containing polymer grafted onto silica particles. *Biomacromolecules* **7**, 1196-1202 (2006).

49 Li, Y., Ding, J., Zhu, J., Tian, H. & Chen, X. Photothermal Effect-Triggered Drug Release from Hydrogen Bonding-Enhanced Polymeric Micelles. *Biomacromolecules* **19**, 1950-1958, doi:10.1021/acs.biomac.7b01702 (2018).

50 Wang, D. *et al.* Supramolecular copolymer micelles based on the complementary multiple hydrogen bonds of nucleobases for drug delivery. *Biomacromolecules* **12**, 1370-1379 (2011).

51 Wu, X., Sacher, E. & Meunier, M. The effects of hydrogen bonds on the adhesion of inorganic oxide particles on hydrophilic silicon surfaces. *J. Appl. Phys.* **86**, 1744-1748, doi:10.1063/1.370956 (1999).

52 Yokoyama, Y. & Yusa, S.-i. Water-soluble complexes formed from hydrogen bonding interactions between a poly (ethylene glycol)-containing triblock copolymer and poly (methacrylic acid). *Polym. J.* **45**, 985-992 (2013).
53 Abebe Alemayehu, Y., Tewabe Gebeyehu, B. & Cheng, C.-C. Photosensitive Supramolecular Micelles with Complementary Hydrogen Bonding Motifs To Improve the Efficacy of Cancer Chemotherapy. *Biomacromolecules* **20**, 4535-4545, doi:10.1021/acs.biomac.9b01322 (2019).
54 Susanti, R., Eti, R. & Tetty, K. in *IOP Conference Series: Earth and Environmental Science.* 012090 (IOP Publishing).
55 Durmus, Z. *et al.* L-lysine coated iron oxide nanoparticles: synthesis, structural and conductivity characterization. *J. Alloys Compd.* **484**, 371-376 (2009).
56 Guo, C. & Holland, G. P. Investigating lysine adsorption on fumed silica nanoparticles. *The Journal of Physical Chemistry C* **118**, 25792-25801 (2014).
57 Villegas, M. F. *et al.* Lysine-Grafted MCM-41 Silica as an Antibacterial Biomaterial. *Bioengineering* **4**, 80 (2017).
58 Iqbal, M. *et al.* Aqueous two-phase system (ATPS): an overview and advances in its applications. *Biological Procedures Online* **18**, 18, doi:10.1186/s12575-016-0048-8 (2016).
59 Shaker Shiran, H., Baghbanbashi, M., Ghazizadeh Ahsaie, F. & Pazuki, G. Study of curcumin partitioning in polymer-salt aqueous two phase systems. *Journal of Molecular Liquids* **303**, 112629, doi:https://doi.org/10.1016/j.molliq.2020.112629 (2020).
60 Sadeghi, R., Hamidi, B. & Ebrahimi, N. Investigation of Amino Acid–Polymer Aqueous Biphasic Systems. *The Journal of Physical Chemistry B* **118**, 10285-10296, doi:10.1021/jp505383r (2014).
61 Noshadi, S. & Sadeghi, R. Evaluation of the capability of ionic liquid–amino acid aqueous systems for the formation of aqueous biphasic systems and their applications in extraction. *The Journal of Physical Chemistry B* **121**, 2650-2664 (2017).
62 Pavlovic, M., Antonietti, M., Schmidt, B. V. K. J. & Zeininger, L. Responsive Janus and Cerberus emulsions via temperature-induced phase separation in aqueous polymer mixtures. *Journal of Colloid and Interface Science* **575**, 88-95, doi:https://doi.org/10.1016/j.jcis.2020.04.067 (2020).
63 Yuan, W. *et al.* Preparation and characterization of recombinant human growth hormone–Zn2+-dextran nanoparticles using aqueous phase–aqueous phase emulsion. *Nanomedicine: Nanotechnology, Biology and Medicine* **8**, 424-427, doi:https://doi.org/10.1016/j.nano.2012.02.007 (2012).
64 Nielen, W. M., Willott, J. D., Esguerra, Z. M. & de Vos, W. M. Ion specific effects on aqueous phase separation of responsive copolymers for sustainable membranes. *Journal of Colloid and Interface Science* **576**, 186-194, doi:https://doi.org/10.1016/j.jcis.2020.04.125 (2020).
65 Dumas, F., Benoit, J.-P., Saulnier, P. & Roger, E. A new method to prepare microparticles based on an Aqueous Two-Phase system (ATPS), without organic solvents. *Journal of Colloid and Interface Science* **599**, 642-649, doi:https://doi.org/10.1016/j.jcis.2021.03.141 (2021).
66 Li, M. & Li, D. Electrically controllable cargo delivery with dextran-rich droplets. *Journal of Colloid and Interface Science* **582**, 102-111, doi:https://doi.org/10.1016/j.jcis.2020.08.033 (2021).
67 Yau, Y. K. *et al.* Current applications of different type of aqueous two-phase systems. *Bioresources and Bioprocessing* **2**, 49, doi:10.1186/s40643-015-0078-0 (2015).
68 Goja, A. M., Yang, H., Cui, M. & Li, C. Aqueous two-phase extraction advances for bioseparation. *J. Bioprocess. Biotechnol* **4**, 1-8 (2013).
69 Wang, X., Wang, G. & Zhang, Y. Research on the biological activity and doxorubicin release behavior in vitro of mesoporous bioactive SiO2-CaO-P2O5 glass nanospheres. *Appl. Surf. Sci.* **419**, 531-539, doi:https://doi.org/10.1016/j.apsusc.2017.05.078 (2017).
70 Karimi, S. & Namazi, H. A photoluminescent folic acid-derived carbon dot functionalized magnetic dendrimer as a pH-responsive carrier for targeted doxorubicin delivery. *New J. Chem.* **45**, 6397-6405 (2021).
71 Tetko, I. V. & Tanchuk, V. Y. Application of Associative Neural Networks for Prediction of Lipophilicity in ALOGPS 2.1 Program. *Journal of Chemical Information and Computer Sciences* **42**, 1136-1145, doi:10.1021/ci025515j (2002).
72 Darani, S. F., Ahsaie, F. G., Pazuki, G. & Abdolrahimi, S. Aqueous two-phase systems based on thermo-separating copolymer for partitioning of doxorubicin. *Journal of Molecular Liquids* **322**, 114542 (2021).
73 Nouri, M., Shahriari, S. & Pazuki, G. Increase of vanillin partitioning using aqueous two phase system with promising nanoparticles. *Scientific Reports* **9**, 19665, doi:10.1038/s41598-019-56120-8 (2019).
74 Mohsen Dehnavi, S., Pazuki, G. & Vossoughi, M. PEGylated silica-enzyme nanoconjugates: a new frontier in large scale separation of α-amylase. *Scientific Reports* **5**, 18221, doi:10.1038/srep18221 (2015).
75 Afzal Shoushtari, B., Rahbar Shahrouzi, J. & Pazuki, G. Effect of Nanoparticle Additives on Partitioning of Cephalexin in Aqueous Two-Phase Systems Containing Poly(ethylene glycol) and Organic Salts. *Journal of Chemical & Engineering Data* **61**, 2605-2613, doi:10.1021/acs.jced.6b00270 (2016).
76 Rangelova, N., Aleksandrov, L. & Nenkova, S. Synthesis and characterization of pectin/SiO2 hybrid materials. *J. Sol-Gel Sci. Technol.* **85**, 330-339, doi:10.1007/s10971-017-4556-z (2018).
77 Agoudjil, N. *et al.* Design and properties of biopolymer–silica hybrid materials: The example of pectin-based biodegradable hydrogels. *Pure Appl. Chem.* **84**, 2521-2529, doi:doi:10.1351/PAC-CON-11-11-18 (2012).
78 Lin, B. & Zhou, S. Poly(ethylene glycol)-grafted silica nanoparticles for highly hydrophilic acrylic-based polyurethane coatings. *Prog. Org. Coat.* **106**, 145-154, doi:https://doi.org/10.1016/j.porgcoat.2017.02.008 (2017).

79 Alexander, S., Gomez, V. & Barron, A. R. Carboxylation and Decarboxylation of Aluminum Oxide Nanoparticles Using Bifunctional Carboxylic Acids and Octylamine. *Journal of Nanomaterials* **2016**, 7950876, doi:10.1155/2016/7950876 (2016).

80 Durmus, Z. *et al.* l-lysine coated iron oxide nanoparticles: Synthesis, structural and conductivity characterization. *J. Alloys Compd.* **484**, 371-376, doi:https://doi.org/10.1016/j.jallcom.2009.04.103 (2009).

81 Ebrahiminezhad, A., Barar, J., Davaran, S., Ghasemi, Y. & Sara, R. Impact of Amino-Acid Coating on the Synthesis and Characteristics of Iron-Oxide Nanoparticles (IONs). *Bull. Korean Chem. Soc.* **33**, 3957-3962 (2012).

82 Nosrati, H., Salehiabar, M., Davaran, S., Danafar, H. & Manjili, H. K. Methotrexate-conjugated L-lysine coated iron oxide magnetic nanoparticles for inhibition of MCF-7 breast cancer cells. *Drug Development and Industrial Pharmacy* **44**, 886-894, doi:10.1080/03639045.2017.1417422 (2018).

83 Liu, X.-Q. *et al.* Temperature induced gelation transition of a fumed silica/PEG shear thickening fluid. *RSC Advances* **5**, 18367-18374, doi:10.1039/C4RA16261G (2015).

84 Catauro, M., Tranquillo, E., Risoluti, R. & Vecchio Ciprioti, S. Sol-Gel Synthesis, Spectroscopic and Thermal Behavior Study of SiO2/PEG Composites Containing Different Amount of Chlorogenic Acid. *Polymers* **10**, doi:10.3390/polym10060682 (2018).

85 P.Krishnamurthi, P., Ramalingam, H. & Raju, K. FTIR studies of hydrogen bonding interaction between the hydroxyl andcarbonyl liquids. *Advances in Applied Science Research* **6** (2015).

86 Li, J., He, L., Liu, T., Cao, X. & Zhu, H. Preparation and characterization of PEG/SiO2 composites as shape-stabilized phase change materials for thermal energy storage. *Sol. Energy Mater. Sol. Cells* **118**, 48-53, doi:https://doi.org/10.1016/j.solmat.2013.07.017 (2013).

87 Guo, L.-M., Xu, X.-M., Zhao, D., Cai, X.-G. & Zhou, B. Biosynthesis, characterization of PLGA coated folate-mediated multiple drug loaded copper oxide (CuO) nanoparticles and it's cytotoxicity on nasopharyngeal cancer cell lines. *AMB Express* **10**, 160, doi:10.1186/s13568-020-01096-2 (2020).

88 Li, X. *et al.* Combination delivery of Adjudin and Doxorubicin via integrating drug conjugation and nanocarrier approaches for the treatment of drug-resistant cancer cells. *J. Mater. Chem. B* **3**, 1556-1564, doi:10.1039/C4TB01764A (2015).

89 Yang, C. *et al.* A facile doxorubicin-dichloroacetate conjugate nanomedicine with high drug loading for safe drug delivery. *Int J Nanomedicine* **13**, 1281-1293, doi:10.2147/IJN.S154361 (2018).

90 Elbialy, N. S., Fathy, M. M. & Khalil, W. M. Doxorubicin loaded magnetic gold nanoparticles for in vivo targeted drug delivery. *Int. J. Pharm.* **490**, 190-199, doi:https://doi.org/10.1016/j.ijpharm.2015.05.032 (2015).

91 Pössel, B. & Mülhaupt, R. Lysine-Functionalized Gibbsite Nanoplatelet Dispersions for Nonisocyanate Polyhydroxyurethane Nanocomposites and Translucent Coatings. *Macromolecular Materials and Engineering* **305**, 2000217, doi:https://doi.org/10.1002/mame.202000217 (2020).

92 El-Mahdy, A. F. M. & Kuo, S.-W. Direct synthesis of poly(benzoxazine imide) from an ortho-benzoxazine: its thermal conversion to highly cross-linked polybenzoxazole and blending with poly(4-vinylphenol). *Polym. Chem.* **9**, 1815-1826, doi:10.1039/C8PY00087E (2018).

93 Zou, Y. *et al.* Synthesis and Solution Processing of a Hydrogen-Bonded Ladder Polymer. *Chem* **2**, 139-152, doi:https://doi.org/10.1016/j.chempr.2016.12.008 (2017).

94 Moussaif, N. *et al.* Mechanically reinforced biodegradable nanocomposites. A facile synthesis based on PEGylated silica nanoparticles. *Polymer* **51**, 6132-6139, doi:https://doi.org/10.1016/j.polymer.2010.10.042 (2010).

95 Hakeem, A. *et al.* Polyaspartic acid-anchored mesoporous silica nanoparticles for pH-responsive doxorubicin release. *Int J Nanomedicine* **13**, 1029 (2018).

96 Li, K. *et al.* Enhanced antitumor efficacy of doxorubicin-encapsulated halloysite nanotubes. *Int J Nanomedicine* **13**, 19 (2018).

97 Manocha, B. & Margaritis, A. Controlled release of doxorubicin from doxorubicin/-polyglutamic acid ionic complex. *Journal of Nanomaterials* **2010**, 780171, doi:10.1155/2010/780171 (2010).

98 Inkson, B. J. in *Materials Characterization Using Nondestructive Evaluation (NDE) Methods* (eds Gerhard Hübschen, Iris Altpeter, Ralf Tschuncky, & Hans-Georg Herrmann) 17-43 (Woodhead Publishing, 2016).

99 Franken, L. E., Boekema, E. J. & Stuart, M. C. A. Transmission Electron Microscopy as a Tool for the Characterization of Soft Materials: Application and Interpretation. *Adv. Sci.* **4**, 1600476, doi:https://doi.org/10.1002/advs.201600476 (2017).

100 An, J., Forchheimer, D., Sävmarker, J., Brülls, M. & Frenning, G. Nanoscale characterization of PEGylated phospholipid coatings formed by spray drying on silica microparticles. *Journal of Colloid and Interface Science* **577**, 92-100, doi:https://doi.org/10.1016/j.jcis.2020.05.045 (2020).

101 Peters, M. *et al.* PEGylating poly(p-phenylene vinylene)-based bioimaging nanoprobes. *Journal of Colloid and Interface Science* **581**, 566-575, doi:https://doi.org/10.1016/j.jcis.2020.07.145 (2021).

102 Purcar, V. *et al.* Preparation and Characterization of Silica Nanoparticles and of Silica-Gentamicin Nanostructured Solution Obtained by Microwave-Assisted Synthesis. *Materials* **14**, 2086 (2021).

103 Smith, J. R., Olusanya, T. O. & Lamprou, D. A. Characterization of drug delivery vehicles using atomic force microscopy: current status. *Expert Opin. Drug Delivery* **15**, 1211-1221 (2018).

104 Cristiano, E., Hu, Y.-J., Siegfried, M., Kaplan, D. & Nitsche, H. A comparison of point of zero charge measurement methodology. *Clays Clay Miner.* **59**, 107-115 (2011).

105 Rafati, A. A., Ebadi, A., Bavafa, S. & Nowroozi, A. Kinetic study, structural analysis and computational investigation of novel xerogel based on drug-PEG/SiO2 for controlled release of enrofloxacin. *Journal of Molecular Liquids* **266**, 733-742, doi:https://doi.org/10.1016/j.molliq.2018.06.104 (2018).

106 Zhu, Y., Fang, Y., Borchardt, L. & Kaskel, S. PEGylated hollow mesoporous silica nanoparticles as potential drug delivery vehicles. *Microporous Mesoporous Mater.* **141**, 199-206, doi:https://doi.org/10.1016/j.micromeso.2010.11.013 (2011).

107 Ahsaie, F. G. & Pazuki, G. Separation of phenyl acetic acid and 6-aminopenicillanic acid applying aqueous two-phase systems based on copolymers and salts. *Scientific reports* **11**, 1-10 (2021).

108 Merchuk, J. C., Andrews, B. A. & Asenjo, J. A. Aqueous two-phase systems for protein separation: Studies on phase inversion. *Journal of Chromatography B: Biomedical Sciences and Applications* **711**, 285-293, doi:https://doi.org/10.1016/S0378-4347(97)00594-X (1998).

109 Sintra, T. E. *et al.* Sequential recovery of C-phycocyanin and chlorophylls from Anabaena cylindrica. *Separation and Purification Technology* **255**, 117538, doi:https://doi.org/10.1016/j.seppur.2020.117538 (2021).

110 Ahsaie, F. G., Pazuki, G., Sintra, T. E., Carvalho, P. & Ventura, S. P. Study of the partition of sodium diclofenac and norfloxacin in aqueous two-phase systems based on copolymers and dextran. *Fluid Phase Equilibria* **530**, 112868 (2021).

111 Aliebrahimi, S., Kouhsari, S. M., Arab, S. S., Shadboorestan, A. & Ostad, S. N. Phytochemicals, withaferin A and carnosol, overcome pancreatic cancer stem cells as c-Met inhibitors. *Biomed. Pharmacother.* **106**, 1527-1536, doi:https://doi.org/10.1016/j.biopha.2018.07.055 (2018).

112 Majdzadeh, M., Aliebrahimi, S., Vatankhah, M. & Ostad, S. N. Effects of celecoxib and L-NAME on apoptosis and cell cycle ofMCF-7 CD44+/CD24-/low subpopulation. *Turkish Journal of Biology* **41**, 826-934 (2017).